Ceramics-Silikáty 60 (3), 210-219 (2016)
journal webpage: www.ceramics-silikaty.cz doi: 10.13168/cs.2016.0032

# COMPARISON OF THERMAL SHOCK BEHAVIOR OF NANO-7YSZ, 15YSZ AND 5.5SYSZ THERMAL BARRIER COATINGS PRODUCED BY APS METHOD

H. JAMALI*, #M.R. LOGHMAN-ESTARKI*, #R. SHOJA RAZAVI*, R. MOZAFARINIA*, H. EDRIS**, S.R. BAKHSHI*

*Department of Materials Engineering, Malek Ashtar University of Technology, P.O. Box 83145/115, Shahin Shahr, Isfahan, Iran
**Department of Materials Engineering, Isfahan University of Technology, Isfahan, P. O. Box. 84156-83111, I. R. Iran

#E-mail: mr.loghman@ma.iut.ac.ir, Shoja_r@yahoo.com

Submitted March 16, 2016; accepted May 10, 2016

**Keywords:** Thermal shock resistance, Atmospheric plasma spraying, Nanostructured thermal barrier coatings

*Nanostructured scandia, yttria doped zirconia (SYSZ), 7 wt. % yttria stabilized zirconia (7YSZ) and 15YSZ thermal barrier coatings (TBCs) were produced by plasma spraying on nickel-based superalloy substrates with NiCrAlY as the bond coat. The thermal shock behavior of the three as-sprayed TBCs at 1000°C was investigated. The results indicated that the thermal cycling lifetime of SYSZ and 7YSZ TBCs was longer than the 15YSZ TBCs due to the lower thermal mismatch stress between the ceramic layer and the metallic layer at high temperature and higher amount of tetragonal phase.*

## INTRODUCTION

Thermally sprayed thermal barrier coatings (TBCs) have been used successfully in gas turbine components to protect the metal parts from hot burner gases. This had led to further increase in operating temperature and some decrease in the amount of cooling air [1-4]. Nowadays, state-of-the-art 7 wt. % yttria stabilized zirconia (7YSZ) is widely used as standard TBC topcoat material [5, 6]. However, the most critical issue for YSZ is the limited operation temperature (< 1250°C) for long term applications. At higher temperature, phase transformations and porous coating sintering result in the formation of cracks in the coating and higher thermal conductivity, accelerate the spallation failure of TBCs [7, 8]. Therefore, investigation of novel TBC materials with ultra-high temperature capability, low thermal conductivity and long-term life time is a key problem for the next generation of turbine engines. Some ceramic materials such as $La_2O_3$–$Y_2O_3$–$ZrO_2$, $Gd_2O_3$–$Y_2O_3$–$ZrO_2$, $La_2Zr_2O_7$, $La_2Ce_2O_7$, $LaMgAl_{11}O_{19}$ and other kinds of rare earth doped zirconia [9-19] have been investigated as potential TBC materials. In recent years, nanostructured zirconia based TBCs deposited by atmospheric plasma spraying have been the focus of attention. It was reported that nanostructured thermal barrier coatings had high bonding strength [20], low thermal conductivity [20-24], and prolonged thermal cycling lifetime [25-27]. Accordingly, nanostructured TBCs are expected to provide better performance than the conventional TBCs.

Recently, codoping YSZ with $Al_2O_3$, $Sc_2O_3$, $Y_2O_3$, $Bi_2O_3$, $Sm_2O_3$, $Yb_2O_3$, $CeO_2$, etc. has attracted researchers to improve thermal and electrical properties of this ceramic [10, 11]. The YSZ had the phase stability up to 1200°C, but upon doping YSZ with scandium oxide (85 - 90 % scandia, 10 - 15 % yttria), the thermal stability of this ceramic was improved up to 1400°C [1, 10]. Increasing the thermal stability of zirconia ceramics can have high potential applications in improving the efficiency and performance of engines [1, 11]. Jang [14] reported that the amount of tetragonal phase was increased by codoping zirconia with scandia and yttria. This was due to the lower amount of scandia was needed for the stabilization of t-zirconia [10, 14]. The strength of the codoped material was almost 10 % higher than that of the reference material (YSZ and ScSZ) [10]. It was also reported that a higher fracture toughness of codoped material was obtained, as compared to the reference material, in accordance with the higher tetragonal phase content and the resulting enhanced transformation toughening [10, 14].

So far, there has been no report on the thermal shock resistance of tetragonal Scandia and yttria codoped zirconia (t-SYSZ) TBC. It is necessary to investigate the thermal shock behavior of SYSZ coatings and the related failure mechanism of them in order to check the possibility of using SYSZ as TBC materials. In this work, tetragonal SYSZ TBCs were sprayed onto Ni-based superalloy by atmospheric plasma spraying. Then, the thermal shock behavior of this coating was compared to the tetragonal 7YSZ and cubic 15YSZ APS coating.

## EXPERIMENTAL

### Materials and Procedures

Thermal barrier coatings, composed of a bond coating and a top coating, were air-plasma-sprayed on a Ni-based superalloy (Inconel 738, Ni–15Cr-8.5Co) substrate. The substrate geometry was a square of 10 × 10 $mm^2$ surface area with 10 mm thickness. The spraying material for the bond coat was commercial Ni22Cr10Al1Y (wt. %, Metco 204NS powder, particle size of 11 to 125 μm) and the top coat were nanostructured scandia-yttria stabilized zirconia (SYSZ, $ZrO_2$– – 0.4 wt. % $Y_2O_3$ 5.1 wt. % $Sc_2O_3$ ) and yttria stabilized zirconia ($ZrO_2$–15 wt. % $Y_2O_3$ and $ZrO_2$–7 wt. % $Y_2O_3$). The ceramic powders of nanostructured 7YSZ (Nanox S4007 powder consisting of agglomerated nanosized particles 15 to 150 μm in diameter) were purchased from Inframat® Advanced Materials™ LLC from USA. The other nanogranules were fabricated in our laboratory from their nanopowders. Because of the poor flow ability of the original nanostructured 15YSZ and SYSZ that made it unsuitable for plasma spraying, these powders had to be agglomerated before spraying. These nanopowders were agglomerated by the sol-gel [1, 2] and spray drying [2, 10] method, respectively. First, a water-soluble binder of 5 wt. % polyvinyl alcohol (PVA) in water at 95°C was prepared. Then, the nanostructured 15YSZ and the organic blinder of PVA were evenly mixed by a stirrer. After that, the mixtures were spray dried using a laboratory spray drier. The main controlled operating parameters were the air temperature at the entry (220 - 235°C), at the exit (135 - 140°C), inside the chamber (180°C), the rotation speed of atomizer (17000 rpm), and the air (4.4 - 4.6 $l \cdot h^{-1}$) and slurry flow rates (1 - 1.2 $kg \cdot h^{-1}$). Finally, semi-spherical and irregular SYSZ agglomerated nanoparticles were obtained. The reason for the obtained morphology by the spray drying method was discussed in our recent paper [2]. The particle size in the range of 20 - 150 μm was chosen for plasma spraying by passing them through a sieve (100 and 500 US mesh). Some specifications of powders are shown in Table 1. Prior to the spraying process, the substrates were successively ground with SiC paper up to 800 (10 μm). They were then cleaned by absolute ethyl alcohol in an ultrasonic set. Before plasma spraying, the substrate was grit blasted by alumina particles with a size of 125 μm. Nanostructured YSZ and SYSZ were sprayed onto the as-sprayed bond coat specimen by an APS system (Plasma-Technik A3000S apparatus, PT Corporation, Switzerland). The APS parameters for depositing bond coat and top coat and their thickness are given in Table 2.

### Thermal shock test

The thermal shock test was carried out in a muffle furnace. When the temperature of the furnace reached 1000°C, the specimens were pushed into the furnace. The specimens were held for about 10 min in the furnace, and then they were directly quenched into water. As the water for the test had a high heat capacity, the temperature rise of water was not obvious. After 60 s, the temperature of specimens was the same as water according to the test of a thermometer contacting the surface of specimens. The temperature of water throughout the cycling was between 23 and 27°C. When the samples were cooled to ambient temperature, they were taken out, dried and put into the high temperature furnace again, repeating the same process. More than 20 % of the cracked and spalled regions of the surface of top coating were defined as the criterion for the failure of the coating. The macroscopic images of the samples in time during the thermal shock test were captured using a digital camera. The weight changes of the samples were measured to a precision of 0.1 mg by an analytical balance (TE214S, Sartorius, Germany). The water-quenched thermal shock test was also performed by other investigations [4, 18].

Table 1. Some specifications of powders used for plasma spraying.

| Type of material | Particle size before and after agglomeration | Morphology | Manufactured method, purchase |
|---|---|---|---|
| 15YSZ | 30-40 nm, 40-120 μm | Semi-spherical | Sol-gel, spray drying and calcination |
| 7YSZ | 75-90 nm, 30-70 μm | Spherical | Inframat company |
| 5.5SYSZ | 40-50 nm, 40-130 μm | Semi-spherical | Sol-gel, spray drying and calcination |
| NiCrAlY | 45-90 μm | Spherical | Sulzer metco, Gas atomized |

Table 2. Plasma spraying parameters and coating thickness.

| Type of material | Top and bond coat thickness (μm) | Current (A), Voltage (V) | Primary gas (Ar), Secondary gas ($H_2$) SLPM* | Carrier gas (Ar) SLPM* | Spray distance (mm), Spray angle (°) | Powder feed rate ($g \cdot min^{-1}$) | Nozzle and injector diameter (mm) |
|---|---|---|---|---|---|---|---|
| 15YSZ | 240 ± 20, 90-110 | 600, 72 | 35, 10 | 3.5 | 120, 90 | 18 | 6, 1.8 |
| 7YSZ | 250 ± 15, 130-140 | 600, 72 | 35, 10 | 3.5 | 120, 90 | 18 | 6, 1.8 |
| 5.5SYSZ | 230 ± 15, 110-120 | 600, 72 | 35, 10 | 3.5 | 120, 90 | 18 | 6, 1.8 |
| NiCrAlY | 45 - 90 (particle size) | 600, 75 | 65, 14 | 2.3 | 120, 90 | 40 | 6, 2.5 |

Coating characterization

The microstructure of as-sprayed coatings was investigated by a field emission scanning electron microscope (FESEM; S-4160, HitachiLtd., Japan). Before taking FESEM images, the sample coated with gold by desk sputter coater (DST3 model, nanostructured coating Co., made in Iran). The phase analysis was carried out by the X-ray diffractometry (XRD; Bruker D8 Advance diffractometer, Germany) with filtered Cu-$K_\alpha$ radiation (0.15406 nm). In order to cater for microstructural and elemental analyses of samples after thermal shock test, scanning electron microscope (Seron Technology-AIS-2000, South Korea) equipped with energy dispersive spectrometer (EDS) was used. The surface roughness (Ra) of substrates prior to spraying was measured by a roughness tester (Mitutoyo SJ-201P, Japan). The measured surface roughness (Ra) of substrates was 9.10 μm. The nanoindenter tester ((*NHTX S/N*: *01-03119*, CSM. Instruments, Geramny) with a Berkovich-type diamond tip was used to determine the elastic modulus (E) of ceramic coatings. In or-

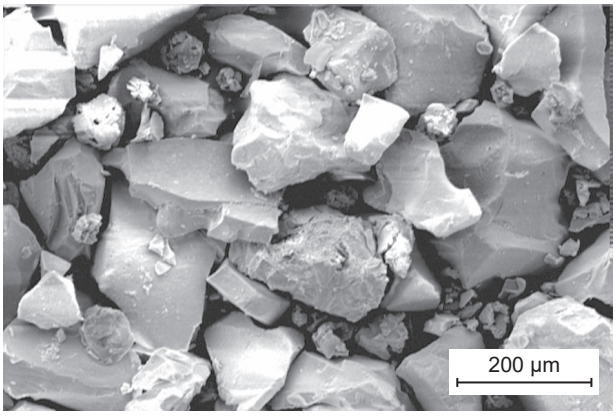


a)

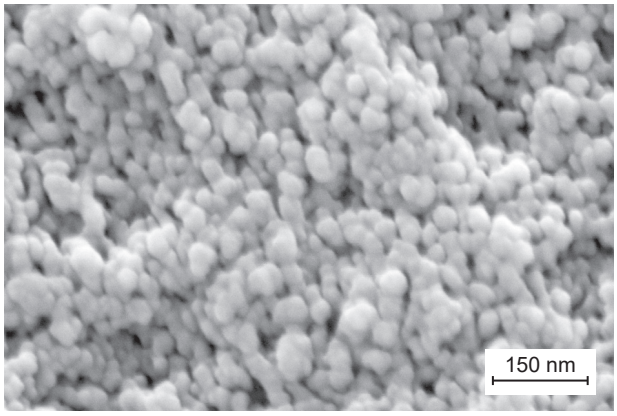


b)

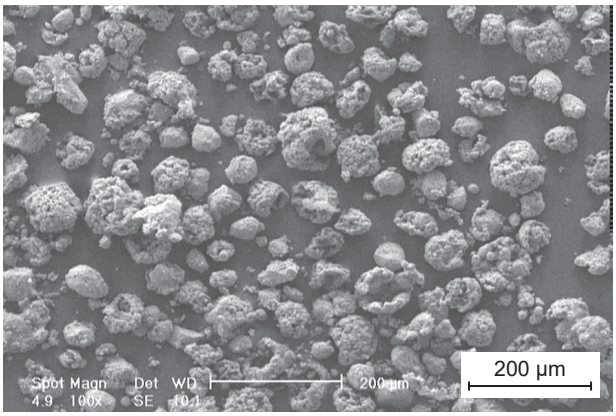


c)

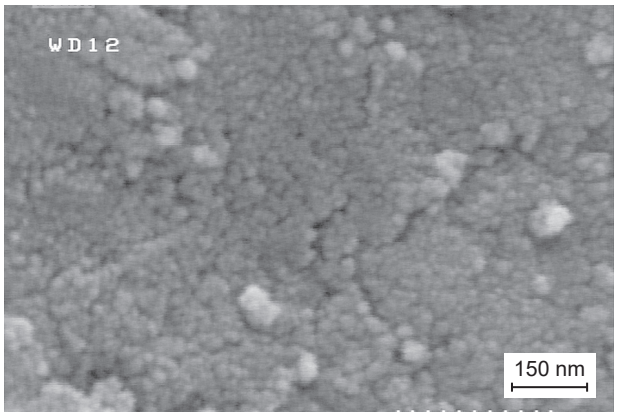


d)

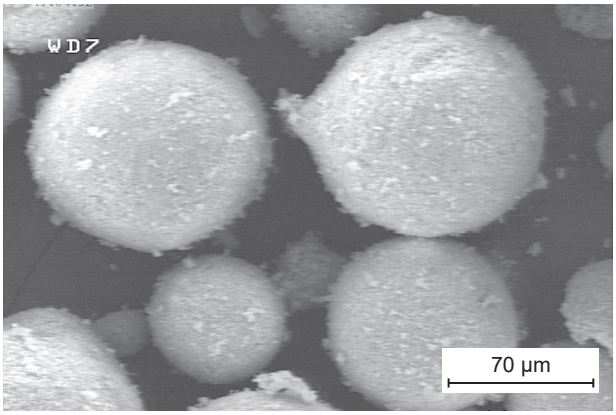


e)

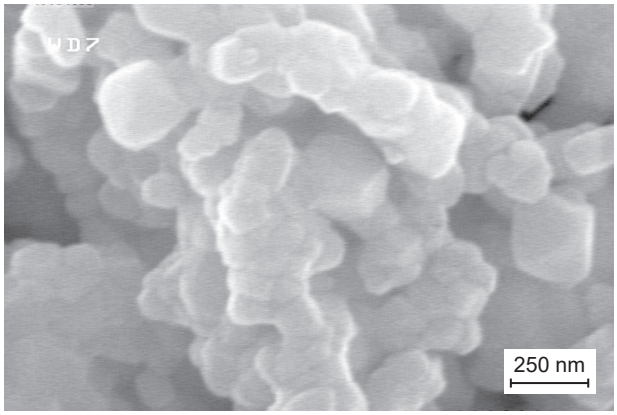


f)

Figure 1. Surface morphology of thermal sprayed feedstock: (a, b) nanostructured laboratory-made 5SYSZ, (c, d) 15YSZ nano-agglomerates, and (e, f) nanostructured 7YSZ feedstock.

der to the indents represent overall coating properties; including dense regions and voids (pores, cracks, unbonded inter-faces), the ten indents was performed randomly on polished cross-section of three coatings. The load used was 10 mN·min$^{-1}$ (20 mN·min$^{-1}$ loading and unloading rate) and the dwell time was 17 s. The percentage of nano-zones (non-melted area) was estimated by image analysis software from SEM images of polished cross sections of samples.

## RESULTS AND DISCUSSION

### Microstructure of the feedstock and its corresponding coating

Figure 1 shows the morphology of the three kinds of feedstocks. From Figure 1a, it is clear that the SYSZ feedstock exhibits polyhedral, irregular and angular shape with different sizes ranging from 20 µm to 130 µm. This may due to obtaining it from sol-gel in the actual process. This affects its flowability and decreases the deposition efficiency. The nanostructured 15YSZ feedstock was composed of spherical/equiaxed shape of nanostructured agglomerates with the size of 30 - 90 µm (Table 1). It can be designated as sphere package structure (Figure 1c). The 7YSZ feedstock had a similar microstructure, but the size distribution was in the range of 20 - 95 µm (Figure 1e).

From the high magnification image of each granule (Figure 1b, d and f), it is clearly observed that their microstructures are composed of nanoparticles with diameter of nearly 40 to 60 nm.

Figure 2 displays the XRD patterns of the three feedstocks and their corresponding coatings. The phase of 15YSZ nano-agglomerate was cubic (Figure 2a), and the corresponding coating was mainly cubic after the plasma spraying process (Figure 2b). The nanostructured 7YSZ feedstock was mainly composed of *t* phase (Figure 2c). The corresponding coating was predicted to be composed of *t′* phase after the plasma spraying (Figure 2d). This tetragonal zirconia phase, which was observed in as-sprayed coating, is mainly composed of the so called non-transformable phase *t′*. It has a lower c and c/a ratio when compared with the t phase (where a, c denote the lattice parameters) [4, 20]. Free yttria (or scandia) was not observed in the XRD pattern of the nanostructured as-sprayed zirconia coatings. It is usually recognized that the t′ phase results from the high-temperature cubic phase by diffusionless transformation at high quenching rate ($10^6$ K·s$^{-1}$). The t phase is the normal tetragonal phase and the content of the $Y_2O_3$ in the *t* phase is lower when compared with the t′ phase.

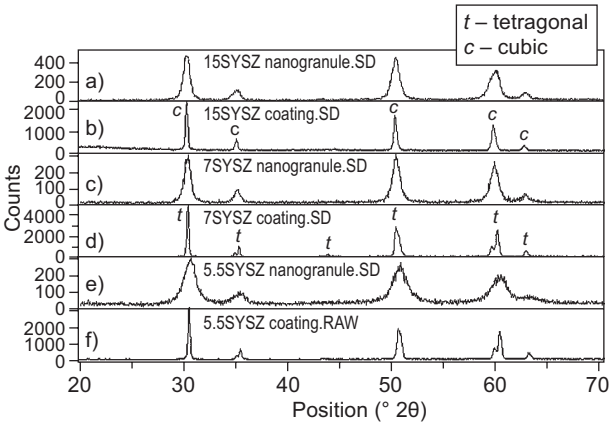


Figure 2. XRD patterns of feedstocks and corresponding APS nanocoatings.

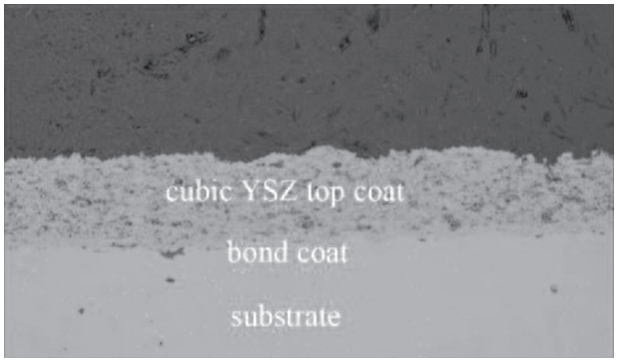


a) 15YSZ

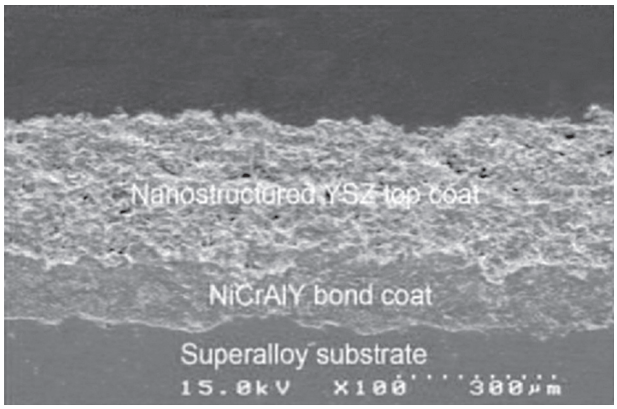


b) 7YSZ

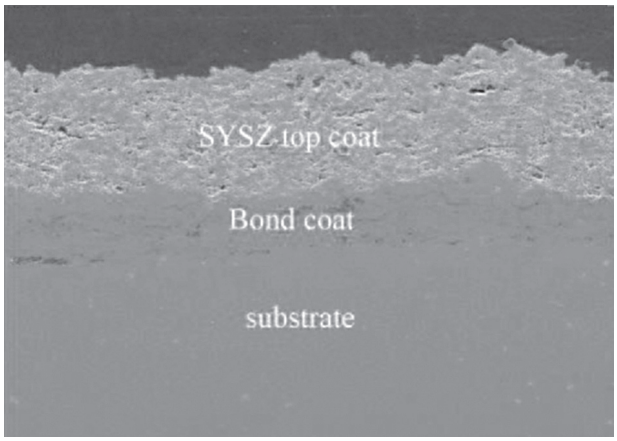


c) 5.5SYSZ

Figure 3. FESEM micrographs of polished cross section of as-sprayed TBC with nanostructured: a) 15YSZ, b) 7YSZ and c) 5.5SYSZ.

The SYSZ nano-agglomerated feedstock formed non-transformable tetragonal phase in the process of spray drying granulation, and the *t′*-phase was kept stable during the plasma spraying, indicating that the phase structure of SYSZ coating was very stable (Figures 2e, f).

Figure 3 presents the polished cross sections of as-sprayed nanostructured TBCs, which are composed of the YSZ or SYSZ top coat and NiCrAlY bond coat deposited on the superalloy substrate by APS process. According to this figure, all three top coatings are well bonded to the bond coating. The fractured cross section morphologies of the three nanostructured coatings are

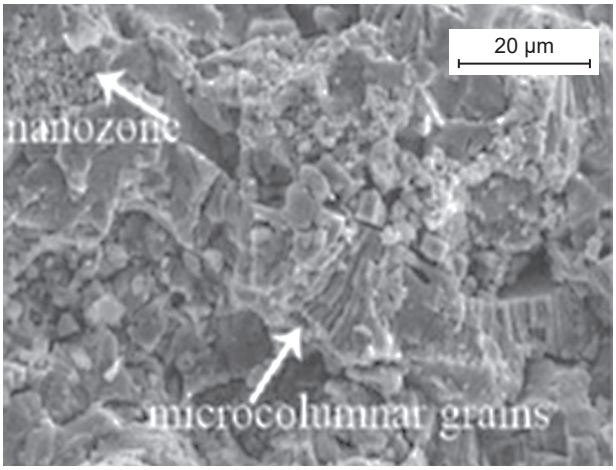


a) 15YSZ

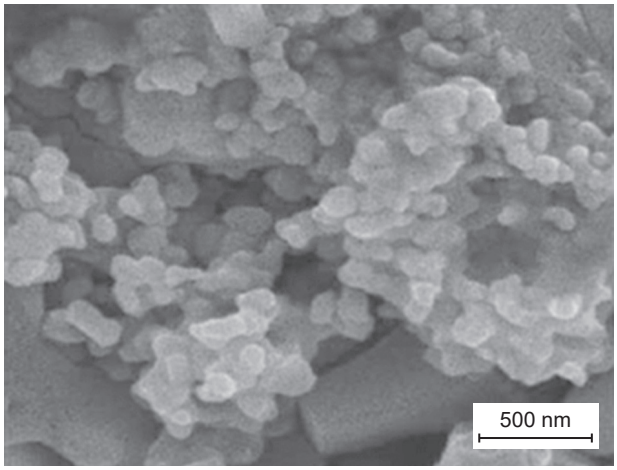


b) 15YSZ

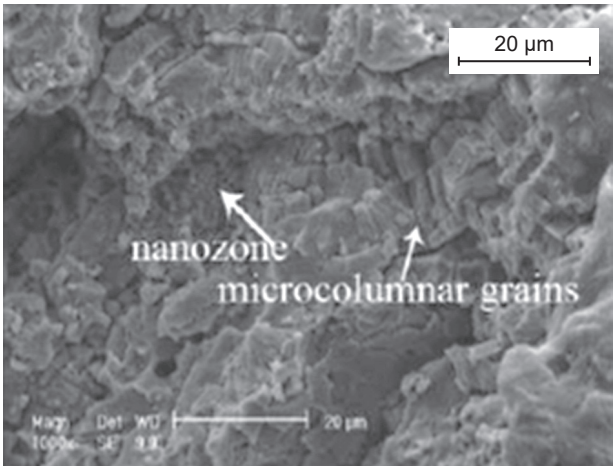


c) 7YSZ

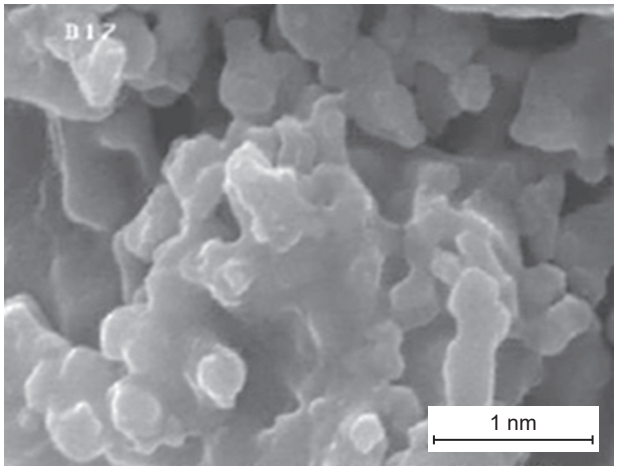


d) 7YSZ

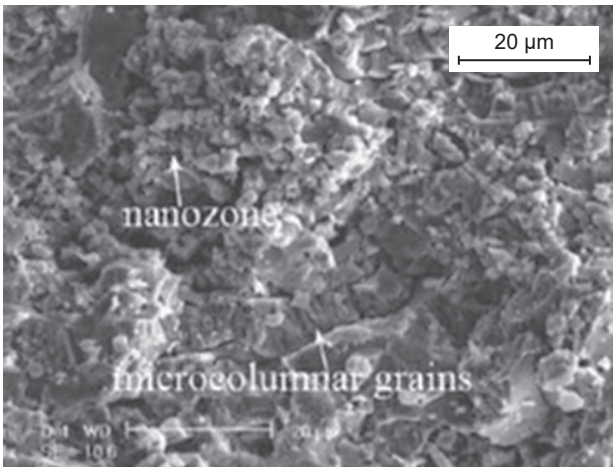


e) 5.5SYSZ

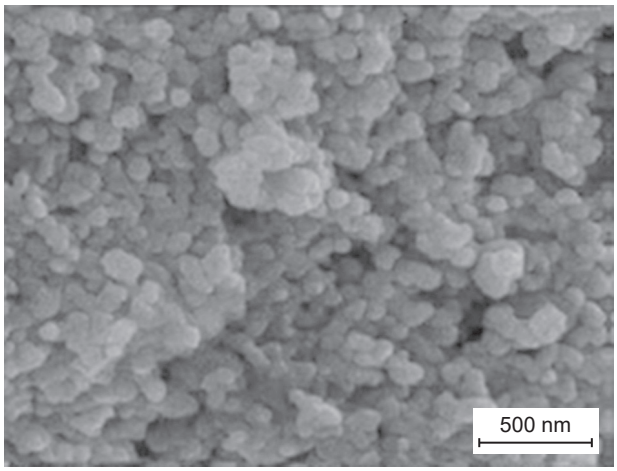


f) 5.5SYSZ

Figure 4. FESEM micrograph of the fractured cross section of as-sprayed nanostructured 15YSZ (a, b), 7YSZ (c, d) and 5.5SYSZ (e, f).

shown in Figure 4. It should be noted that two types of microstructure are present in all nanostructured coatings (Figure 4): The columnar grains were solidified from the melted fraction of YSZ (or SYSZ) powder and the loose microstructure was retained from the unmelted YSZ (or SYSZ) powder [2, 4, 20]. Therefore, all three coatings exhibited a bimodal microstructure consisting of nanosized particles retained from the powder and microcolumnar grains formed through the solidification of the melted fraction in spray particles. The percentage of nano-zones embedded in the 7YSZ and 15YSZ coating structure was approximately 25 ± 2 %. The SYSZ coating showed the lower percentage of partially melted area (nanozone, 19 ± 3 %) due to the different degree of melting irregular particle feedstocks in comparison with spherical particle feedstocks [2, 20]. The nanozones contained a large volume fraction of pores with sizes ranging from several tens to several hundreds of nanometers. This porous structure enhances the thermal insulation effect of TBCs [16-20].

## Thermal shock behaviors of TBCs

Figure 5 shows macroscopic images of the nanostructured TBCs during thermal shock testing. In order to consider "edge effects" in the practical application of thermal barrier coatings, such as edges and corners in combustor and blade rim, square specimens were used. As can be seen, for all coatings, failure starts from the edges of the sample and then propagates to the adjacent areas. Beginning of the failure from the edges was due to the extreme heating and cooling conditions encountered and the singularity of thermal stresses at the edges. Other studies [4, 26, 27] have also mentioned the edge effect on failure during thermal cycling.

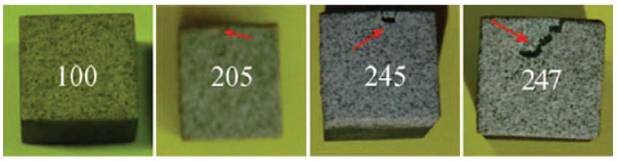


a) SYSZ

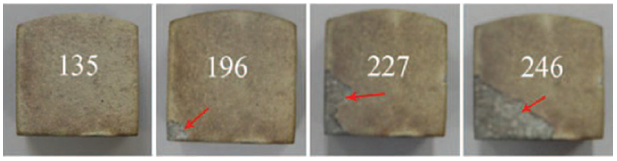


b) 7YSZ

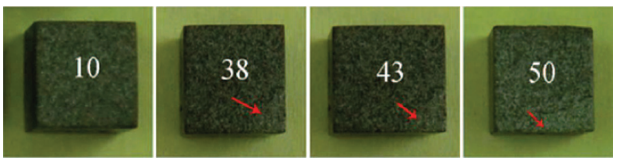


c) 15YSZ

Figure 5. Photographs of nanostructured: a) SYSZ, b) 7YSZ and c) 15YSZ samples during thermal shock testing.

Figure 6 presents the weight changes as a function of cycle number for three kinds of nanostructured samples during thermal shock testing. Based on this figure, the nanostructured *t*-7YSZ and *t*-5.5SYSZ coatings, as compared to *c*-15YSZ, exhibited a better performance during thermal shock testing. As can be seen, the weight of all samples first increased due to substrate

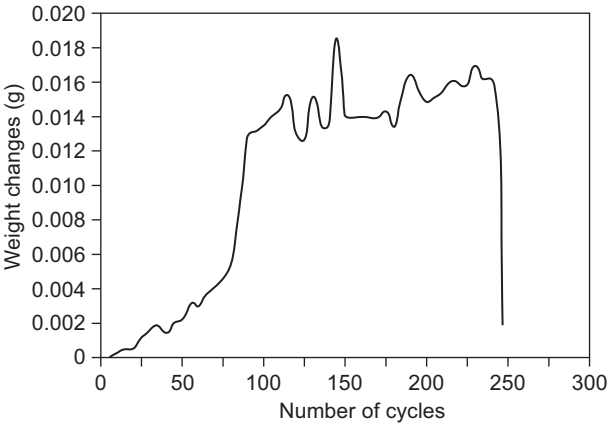


a) 15YSZ

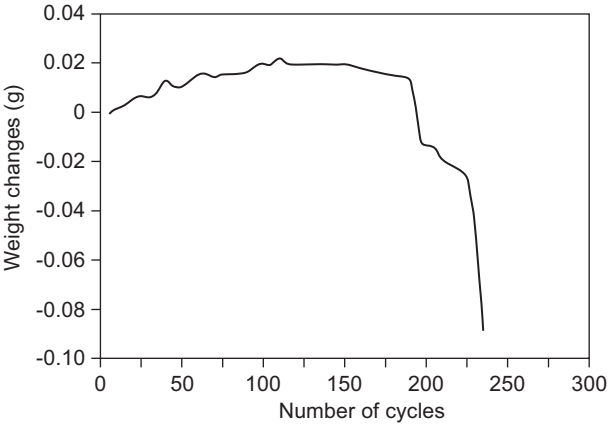


b) 7YSZ

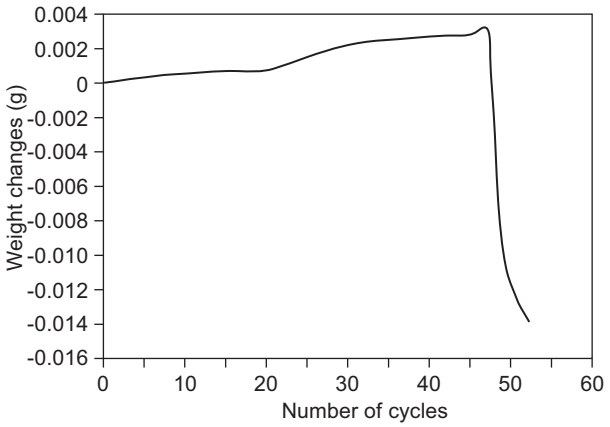


c) 5.5SYSZ

Figure 6. Weight change as a function of cycle number for: a) SYSZ, b) 7YSZ and c) 15YSZ TBCs during thermal shock testing.

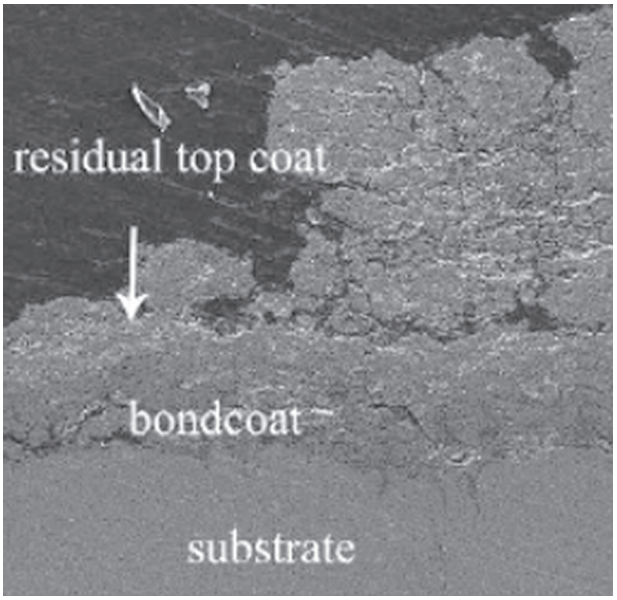


a) SYSZ

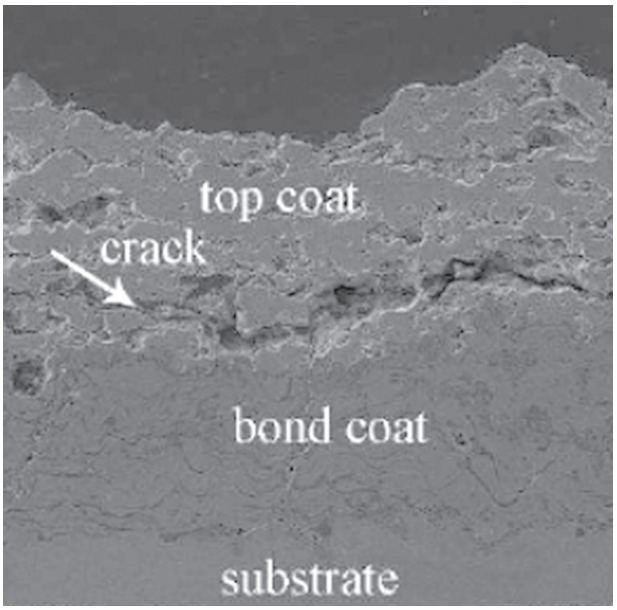


b) 7YSZ

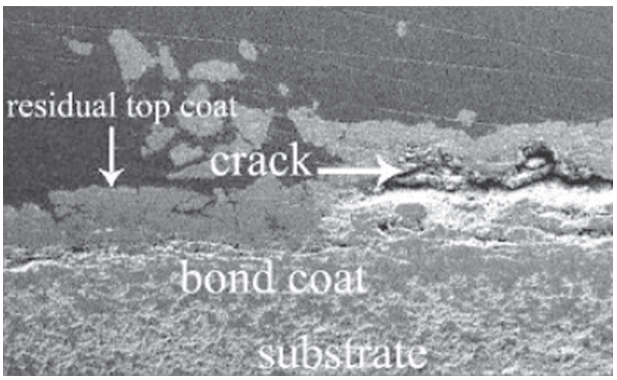


c) 15YSZ

Figure 7. SEM micrographs of polished cross section of nanostructured: a) SYSZ, b) 7YSZ and c) 15YSZ TBCs after 247, 246 and 50 cycles, respectively.

free surface oxidation and then reduced suddenly after some cycles. After sudden weight loss, a weight gain was observed that could be due to both substrate and bond coat oxidation. Since gradual weight loss was not observed, coatings delaminations did not occur. On the other hand, the sudden weight loss of samples implied that coatings spallation could occur.

The polished cross sections of the nanostructured 15YSZ, 7YSZ and 5.5SYSZ TBCs after thermal shock testing are shown in Figure 7. As can be seen, in all coatings cracks were initiated within the ceramic top coat near the top coat/bond coat interface. Based on this figure, the lack of thickness loss of both coatings during thermal shock also refuted the coating delamination mechanism. Therefore, analysis of weight changes (Figure 6) and microscopic images (Figure 7) showed that the failure of the three nanostructured coatings was in a similar mode, occurring as spallation of the top coat, near and parallel to the top coat/bond coat interface. Research shows that after thermal shock tests, four types of cracks were formed in the TBCs, namely, vertical cracks, horizontal cracks, propagating cracks, and penetrating cracks [23]. In penetrating cracks, vertical cracks penetrate the bond coat to the substrate surface. In the current work, after thermal cycles, vertical and propagating or horizontal crack emerged in the SYSZ and YSZ top coat (Figure 7). However, no obvious oxide and the penetrating crack were generated at the bond coat and the substrate interface, in contrast to what was formed in Li work [23] on thermal failure of nanostructured TBCs.

Previous studies [27-29] showed that oxidation of the bond coat and thermal mismatch stress were the main factors causing degradation of TBCs. EDS analyses of top coat/bond coat interfaces of the three nanostructured TBCs after thermal shock testing are shown in Figure 8. Based on this analysis, for all coatings, thermally grown oxide (TGO) was not formed on the top coat/bond coat interface. The SEM micrographs of samples after thermal shock testing (Figure 7) also confirm the absence of TGO formation. Therefore, it can be concluded that bond coat oxidation did not occur during thermal cycling, thereby not contributing to the coating failure. It seems that the absence of visible TGO formation is due to short heating time [29, 30].

Figure 9 presents the XRD patterns of nanostructured TBCs coatings after failure. According to the XRD patterns (Figure 9a, b), the as-sprayed 5.5SYSZ and 7YSZ coatings were completely made of a non-transformable tetragonal (t´) phase. In the case of 15YSZ, Figure 9c shows that c-phase was decomposed to cubic and (transformable) tetragonal phase. After long-term thermal cycling, the metastable transformable tetragonal phase may be decomposed into low-stabilizer tetragonal phase by the diffusion of the stabilizer ($Y_2O_3$ or $Sc_2O_3$), and the low-stabilizer tetragonal phase may be transformed into monoclinic phase. The tetragonal-to-monoclinic phase transformation is martensitic in nature

and it is accompanied by a significant volume increase of approximately 3 - 5 vol. %, affecting the integrity of the coating [4, 28-30]. Anyway, in this study, no phase change was observed during the thermal shock of SYSZ and 7YSZ coatings. Accordingly, stresses resulting from phase transformation made no contribution to the degradation of both coatings. In layered systems, the coefficient of thermal expansion is an important property because the thermal stress resulting from the coefficient of thermal expansion (CTE, α) mismatch between the layers may lead to degradation. Therefore, CTE mismatch can be one of the key factors responsible for the failure of TBCs.

The substrate and bond coat, due to similar chemical compositions, have low CTE mismatch. But, since the difference in CTE between the ceramic top coat and the underlying metallic components is high, it could be anticipated that top coat/bond coat interface stresses would be high upon heating/cooling of the substrate/coating system. Therefore, thermal stresses caused by the mismatch of the thermal expansion are concentrated at the interface between ceramic top coat and metallic bond coat. With continuous exposure of samples to thermal cycles, these stresses result in crack nucleation and propagation in the ceramic top coat. Later, these initial cracks can assiste each other and with propagation in the top coat, near and parallel to top coat/bond coat interface, finally resulte in top coat spallation. Therefore, during thermal shock testing, the failures of all nanostructured SYSZ, 7YSZ and 15YSZ coatings were dominated by thermal stresses generated due to the difference in CTE between the ceramic top coat and the underlying metallic components. The crack formation and propagation in the top coat and the remaining little parts of top coat on the bond coat (Figure 7) also confirm this conclusion.

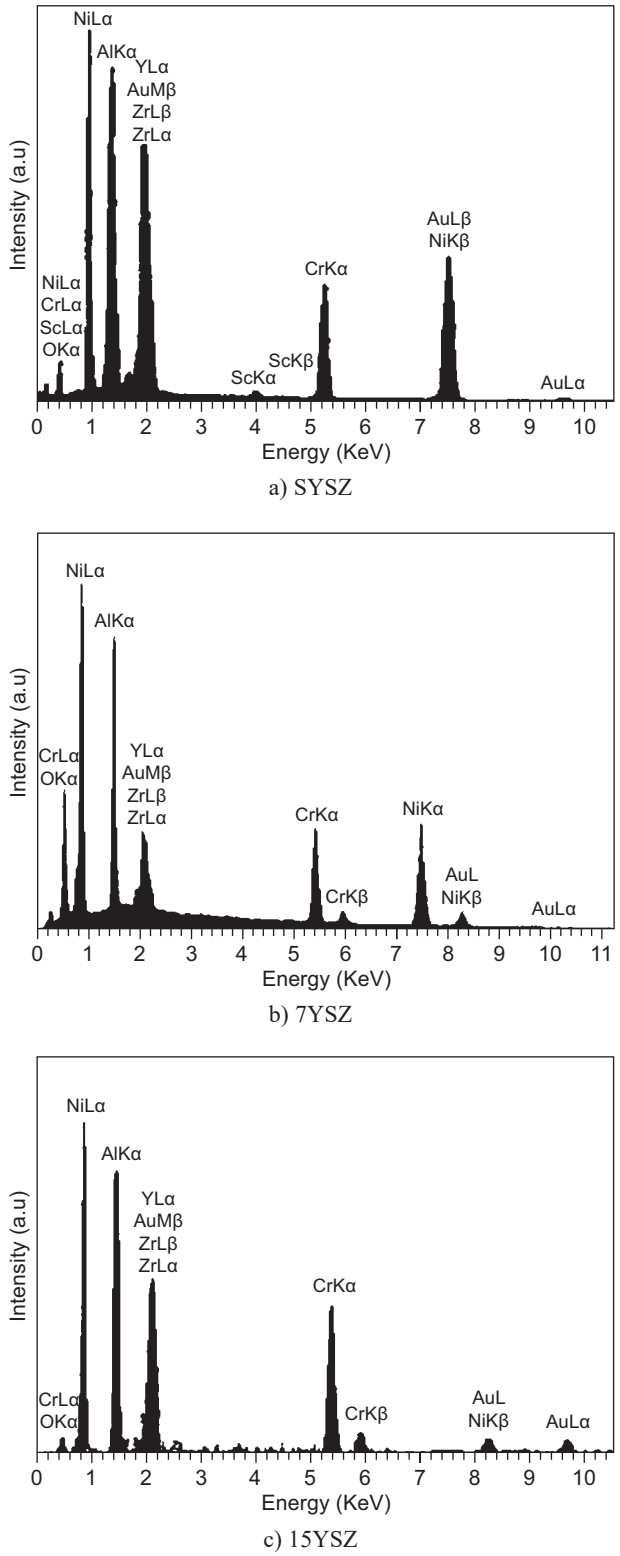


Figure 8. EDS analyses from top coat/bond coat interface of nanostructured: a) SYSZ, b) 7YSZ and c) 15YSZ TBCs after failure.

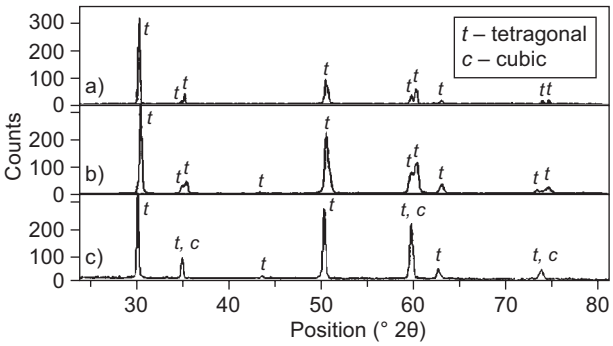


Figure 9. XRD patterns of nanostructured: a) SYSZ, b) 7YSZ and c) 15YSZ coatings after thermal shock testing.

## Thermal shock lifetime

Thermal shock resistance depends on the size and distribution of pores or existing cracks in the coating. Thermal cycling can result in the cracking and spalling of TBC. It is due to the fact that cyclic thermal loads can cause horizontal or vertical cracks to propagate, resulting in delamination/spallation of the coating and loss of thermal protection to the substrate. The thermal

cycling lifetimes of the three nanostructured TBCs are graphically presented in Figure 10. It can be seen that the nanostructured 7YSZ and SYSZ TBCs exhibit an excellent average thermal cycling lifetime, approximately 5 times higher than that of the 15YSZ TBC.

When the coating specimen was taken out from the high temperature furnace and quickly quenched in water in the process of thermal cycling, a very large stress was developed in the coating due to the difference of thermal expansion coefficients between the ceramic layer and the metallic substrate, which can be given by the following expression:

$$\sigma_c = \Delta\alpha \cdot \Delta T \cdot E/(1 - \nu^2) \quad (1)$$

where $\sigma_c$ is the developed stress in the coating, and $E$ and $\nu$ are Young's modulus and Poisson ratio of the ceramic coating, respectively. $\Delta\alpha$ is the difference in CTE between the ceramic coating and the metallic substrate, and $\Delta T$ is the change in temperatures. The $\alpha$ coefficient of Inconel 738 Ni-based substrate, plasma-sprayed NiCrAlY bond coat, and plasma-sprayed top coat at 1000°C is reported as $17.5 \times 10^{-6}$ °C$^{-1}$ [3], $15 \times 10^{-6}$ °C$^{-1}$ [3] and $11.7 \times 10^{-6}$ °C$^{-1}$ (7YSZ), $11.5 \times 10^{-6}$ °C$^{-1}$ (SYSZ), $10.53 \times 10^{-6}$ °C$^{-1}$ (15YSZ) [3, 23], respectively. By taking Poisson ratio and elastic modulus value equal to 0.12 and 26 GPa, the thermal expansion mismatch stress value ($\sigma_c$) of 7YSZ, SYSZ and 15YSZ was obtained to be 0.142 GPa, -0.147 GPa and -0.170 GPa, respectively. This result shows that 15YSZ sustains more CTE stress than SYSZ and 7YSZ TBCs. Furthermore, the elastic modulus of t-7YSZ (161.5 GPa) and t-SYSZ (186.00 GPa) coatings, as compared to the 15YSZ (205.70 GPa) coating, was lower. This caused an increase in the compliance capabilities and thermal relaxation of their coatings as compared to its c-15YSZ counterpart. Since the CTE of the metallic substrate and bond coat, as compared to the ceramic topcoat, is very high, a larger CTE of the top coat means a lower thermal mismatch between the topcoat and bond coat layers. Thus, it can be expected that the main factor in TBC failure, i.e., the thermal stress generated during the thermal cycling, is lower for nanostructured tetragonal 7YSZ and SYSZ coatings, as compared to the cubic 15YSZ

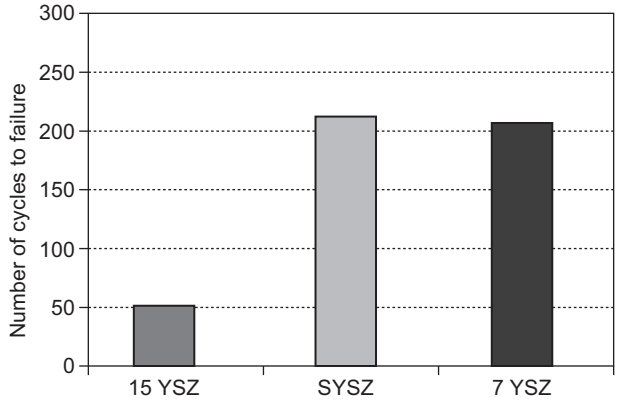


Figure 10. The thermal cycling life times of the three nanostructured TBCs.

Comparison of weight change curves (Figure 6) shows that the failure (a destruction of more than 20 % in the coating surface) of nanostructured tetragonal 7YSZ and SYSZ TBCs, as compared to the cubic 15YSZ TBC, has occurred in several stages. Based on 7YSZ and SYSZ coatings, a smaller surface of the coating is degraded in each stage than in the 15YSZ coating.

## CONCLUSIONS

The reliable performance of TBCs is a very important topic in the industry. Since the contribution of these coatings in turbine engine efficiency is undeniable, their durability against high temperature thermal cycles is very important. Therefore, the thermal shock resistance of plasma-sprayed nanostructured SYSZ, 7YSZ and 15YSZ TBCs was investigated in a comparative aspect.

The major conclusions are as follows:

- In all cases, the initial cracks were generated at the corner of the square specimen.
- The failures of three nanostructured TBCs were due to the spallation of top coat, near and parallel to top coat/ /bond coat interface. The thermal stress caused by the difference in CTE between the ceramic top coat and the underlying metallic components was identified as the major factor of TBC failure.
- The thermal cycling lifetime of 5.5SYSZ and 7YSZ TBCs was 5 times higher than the 15YSZ TBCs due to the lower thermal mismatch stress between the ceramic layer and the metallic layer at 1000°C and higher amount of tetragonal phase.

## Acknowledgments

*The authors would also like to thank M. Hajizadeh-Oghaz, Mr. Mahmoudi and Zia Valefi for their cooperation.*

## REFERENCES

1. Leoni M., Jones R. L., Scardi P. (1998): Phase stability of scandia–yttria-stabilized zirconia TBCs. *Surface and coatings technology*, *108*, 107-113. doi:10.1016/S0257-8972(98)00617-3
2. Loghman-Estarki M.R., Edris H., Jamali H., Ghasemi R., Pourbafrany M., Erfanmanesh M., Ramezani M. (2013): Spray drying of nanometric SYSZ powders to obtain plasma sprayable nanostructured granules. *Ceramics International*, *39*(8), 9447-9457. doi:10.1016/j.ceramint.2013.05.062
3. Lima C.R.C., Guilemany J.M. (2007): Adhesion improve-

ments of thermal barrier coatings with HVOF thermally sprayed bond coats. *Surface and Coatings Technology*, *201*(8), 4694-4701. doi:10.1016/j.surfcoat.2006.10.005

4. Jamali H., Mozafarinia R., Shoja Razavi R., Ahmadi-Pidani R., Reza Loghman-Estarki, M. (2012): Fabrication and evaluation of plasma-sprayed nanostructured and conventional YSZ thermal barrier coatings. *Current Nanoscience*, *8*(3), 402-409. doi:10.1016/j.ceramint.2012.05.060
5. Hong Z., Fei L., Bo H., Jun W., Sun, B.D. (2007): Nanostructured yttria stabilized zirconia coatings deposited by air plasma spraying. *Transactions of Nonferrous Metals Society of China*, *17*(2), 389-393. doi:10.1016/S1003-6326(07)60104-6
6. Wang L., Wang Y., Sun X.G., He J.Q., Pan Z. Y., Wang C.H. (2012): Thermal shock behavior of 8YSZ and double-ceramic-layer La 2 Zr 2 O 7/8YSZ thermal barrier coatings fabricated by atmospheric plasma spraying. *Ceramics International*, *38*(5), 3595-3606. doi:10.1016/j.ceramint.2011.12.076
7. Sobhanverdi R., Akbari A. (2015): Porosity and microstructural features of plasma sprayed Yttria stabilized Zirconia thermal barrier coatings. *Ceramics International*, *41*(10), 14517-14528. doi:10.1016/j.ceramint.2015.07.102
8. Zhu D., Miller R.A. (1998): Sintering and creep behavior of plasma-sprayed zirconia-and hafnia-based thermal barrier coatings. *Surface and Coatings Technology*, *108*, 114-120. doi:10.1016/s0257-8972(98)00669-0
9. Matsumoto M., Yamaguchi N., Matsubara H. (2004): Low thermal conductivity and high temperature stability of $ZrO_2$–$Y_2O_3$–$La_2O_3$ coatings produced by electron beam PVD. *Scripta Materialia*, *50*(6), 867-871. doi:10.1016/j.scriptamat.2003.12.008
10. Loghman-Estarki M.R., ShojaRazavi R., Edris H. (2012): Synthesis of SYSZ nanocrystal via new wet chemical method. *Current Nanoscience*, *8*, 767. doi: 10.2174/157341312802884364
11. Vassen R., Cao X., Tietz F., Basu D., Stöver D. (2000): Zirconates as new materials for thermal barrier coatings. *Journal of the American Ceramic Society*, *83*(8), 2023-2028. doi:10.1111/j.1151-2916.2000.tb01506.x
12. Vassen R., Cao X., Tietz F., Basu D., Stöver D. (2000): Zirconates as new materials for thermal barrier coatings. *Journal of the American Ceramic Society*, *83*(8), 2023-2028. doi:10.1002/adma.200304132
13. Friedrich C., Gadow R., Schirmer T. (2001): Lanthanum hexaaluminate – a new material for atmospheric plasma spraying of advanced thermal barrier coatings. *Journal of thermal spray technology*, *10*(4), 592-598. doi:10.1002/adma.200304132
14. Xu G., Zhang Y.W., Han B., Li M.J., Li C., Yan C.H. (2003): Unusual calcination temperature dependent tetragonal–monoclinic transitions in rare earth-doped zirconia nanocrystals. *Physical Chemistry Chemical Physics*, *5*(18), 4008-4014. doi:10.1039/b304966c
15. Guo H., Zhang H., Ma G., Gong S. (2009): Thermophysical and thermal cycling properties of plasma-sprayed $BaLa_2Ti_3O_{10}$ coating as potential thermal barrier materials. *Surface and Coatings Technology*, *204*(5), 691-696. doi:10.1016/j.surfcoat.2009.09.009
16. Zisis T., Fleck N. A. (2010): The elastic–plastic indentation response of a columnar thermal barrier coating. *Wear*, *268*(3), 443-454. doi:10.1016/j.wear.2009.08.035
17. Xie X.Y., Guo H.B., Gong S. K. (2010): Mechanical properties of LaTi2Al9O19 and thermal cycling behaviors of plasma-sprayed $LaTi_2Al_9O_{19}$/YSZ thermal barrier coatings. *Journal of thermal spray technology*, *19*(6), 1179-1185. doi:10.1007/s11666-010-9529-5
18. Steinbrech R.W., Postolenko V., Mönch J., Malzbender J., Singheiser L. (2011): Testing method to assess lifetime of EB-PVD thermal barrier coatings on tubular specimens in static and cyclic oxidation tests. *Ceramics International*, *37*(1), 363-368. doi: 10.1016/j.ceramint.2010.09.028
19. Bratton R.J., Lau S.K., Lee, S.Y. (1980): Evaluation of present-day thermal barrier coatings for industrial/utility applications. *Thin Solid Films*, *73*(2), 429-437. doi:10.1016/ 0040-6090(80)90511-8
20. Jamali H., Mozafarinia R., Shoja Razavi R., Ahmadi-Pidani R., Reza Loghman-Estarki M. (2012). Fabrication and evaluation of plasma-sprayed nanostructured and conventional YSZ thermal barrier coatings. *Current Nanoscience*, *8*(3), 402-409. doi:10.2174/ 157341312800620250
21. Brandl W., Grabke, H.J., Toma D., Krüger J. (1996): The oxidation behaviour of sprayed MCrAlY coatings. *Surface and Coatings Technology*, *86*, 41-47. doi:10.1016/s0257-8972(96)03039-3
22. Mayoral M.C., Andrés J.M., Bona M.T., Higuera V., Belzunce F. J. (2008): Aluminium depletion in NiCrAlY bond coatings by hot corrosion as a function of projection system. *Surface and Coatings Technology*, *202*(9), 1816-1824. doi:10.1016/j.surfcoat.2007.07.068
23. Zhou C., Zhang Q., Li Y. (2013): Thermal shock behavior of nanostructured and microstructured thermal barrier coatings on a Fe-based alloy. *Surface and Coatings Technology*, *217*, 70-75. doi:10.1016/j.surfcoat.2012.11.074
24. Miller R.A. (1987): Current status of thermal barrier coatings – an overview. *Surface and Coatings Technology*, *30*(1), 1-11. doi:10.1016/0257-8972(87)90003-x
25. Ramachandra C., Lee K.N., Tewari S.N. (2003): Durability of TBCs with a surface environmental barrier layer under thermal cycling in air and in molten salt. *Surface and Coatings Technology*, *172*(2), 150-157. doi:10.1016/s0257-8972(03)00260-3
26. Ahmadi-Pidani R., Shoja-Razavi R., Mozafarinia R., Jamali H. (2012): Improving the thermal shock resistance of plasma sprayed CYSZ thermal barrier coatings by laser surface modification. *Optics and Lasers in Engineering*, *50*(5), 780-786. doi:10.1016/j.optlaseng.2011.12.007
27. Giolli C., Scrivani A., Rizzi G., Borgioli F., Bolelli G., Lusvarghi L. (2009): Failure mechanism for thermal fatigue of thermal barrier coating systems. *Journal of thermal spray technology*, *18*(2), 223-230. doi:10.1007/s11666-009-9307-4
28. Khan A.N., Lu J. (2007): Thermal cyclic behavior of air plasma sprayed thermal barrier coatings sprayed on stainless steel substrates. *Surface and Coatings Technology*, *201*(8), 4653-4658. doi:10.1016/j.surfcoat.2006.10.022
29. Liu Y., Persson C., Wigren J. (2004): Experimental and numerical life prediction of thermally cycled thermal barrier coatings. *Journal of thermal spray technology*, *13*(3), 415-424. doi:10.1361/10599630420399
30. Ahmaniemi S., Vuoristo P., Mäntylä T., Gualco C., Bonadei A., Di Maggio R. (2005): Thermal cycling resistance of modified thick thermal barrier coatings. *Surface and Coatings Technology*, *190*(2), 378-387. doi:10.1016/j.surfcoat.2004.02.028